# Topological Spin Excitations in Non-Hermitian Spin Chains with a Generalized Kernel Polynomial Algorithm

Guangze Chen,[1] Fei Song,[2,*] and Jose L. Lado[1,†]
[1]Department of Applied Physics, Aalto University, 02150 Espoo, Finland
[2]Institute for Advanced Study, Tsinghua University, Beijing 100084, China

(Received 18 August 2022; revised 9 December 2022; accepted 6 February 2023; published 7 March 2023)

Spectral functions of non-Hermitian Hamiltonians can reveal the existence of topologically nontrivial line gaps and the associated topological edge modes. However, the computation of spectral functions in a non-Hermitian many-body system remains an open challenge. Here, we put forward a numerical approach to compute spectral functions of a non-Hermitian many-body Hamiltonian based on the kernel polynomial method and the matrix-product state formalism. We show that the local spectral functions computed with our algorithm reveal topological spin excitations in a non-Hermitian spin model, faithfully reflecting the nontrivial line gap topology in a many-body model. We further show that the algorithm works in the presence of the non-Hermitian skin effect. Our method offers an efficient way to compute local spectral functions in non-Hermitian many-body systems with tensor networks, allowing us to characterize line gap topology in non-Hermitian quantum many-body models.

DOI: 10.1103/PhysRevLett.130.100401

Non-Hermitian (NH) Hamiltonians have risen as a rich framework to describe the postselected quantum dynamics of open quantum systems [1–3]. NH Hamiltonians have been found to host a variety of phenomena lacking a counterpart in Hermitian systems, including the non-Hermitian skin effect (NHSE) [4–12]. In addition, NH Hamiltonians exhibit unique topological properties: a topologically nontrivial gap can either be a line gap or a point gap [13–15]. The line gap is a generalization of the spectral gap in Hermitian systems, and a topologically nontrivial line gap is associated with topological edge modes in open boundary conditions [14]. The point gap topology is unique for non-Hermitian systems and it encodes the origin of the NHSE [16–18]. Recently, the generalization of NH topology as well as other interesting aspects of NH physics such as parity-time symmetry breaking [19–21] and exceptional points [22–25] to NH many-body systems have attracted much interest [26–30].

Despite the intense interest in the study of NH many-body physics, efficient numerical tools are lacking. In the case of interacting one-dimensional problems, conventional tools to study Hermitian many-body systems based on the density matrix renormalization group (DMRG) [31] cannot be directly applied to study NH many-body systems. In Hermitian many-body systems, local spectral functions can be computed efficiently for large-size systems within the DMRG framework using correction vector methods [32,33], time evolution [34,35], or kernel polynomial algorithms [36–38]. However, for NH many-body Hamiltonians, the kernel polynomial method (KPM) does not apply directly [39], and an efficient algorithm to compute local spectral functions in NH many-body systems is lacking. The computation of local spectral functions of many-body excitations allows revealing many-body topological modes [38], and therefore would be of key interest to address topological interacting NH many-body models, in particular with a nontrivial line gap.

Here, we put forward a many-body non-Hermitian kernel polynomial method (NHKPM) [40] to compute local spectral functions in NH many-body systems. We implement a KPM-based algorithm to compute the local spectral functions, where matrix-product states (MPSs) are used to represent the states. We show that this method reveals topological many-body spin excitations in a NH spin chain with nontrivial line gap topology. We further show that this method provides faithful results in the presence of the NHSE. Our results put forward a many-body algorithm to efficiently compute spectral functions in NH many-body systems, which in particular allows us to characterize line gap topology in NH many-body systems.

We first summarize how the KPM is used to compute local spectral functions in Hermitian spin systems. For a Hermitian $S = 1/2$ Hamiltonian $H_0$, the local spectral density of $S_z = \pm 1$ excitations is given by the local spin structure factor

$$\rho(E, l) = \langle \mathrm{GS}|S_l^- \delta(E + E_{\mathrm{GS}} - H_0) S_l^+|\mathrm{GS}\rangle + \langle \mathrm{GS}|S_l^+ \delta(E + E_{\mathrm{GS}} - H_0) S_l^-|\mathrm{GS}\rangle \quad (1)$$

where $|\mathrm{GS}\rangle$ and $E_{\mathrm{GS}}$ are the ground state and its energy, and $S_l^{\pm} = S_l^x \pm i S_l^y$ where $l$ is the site index. Such a local spin structure factor reveals topological spin excitations [38], which can be probed with scanning tunneling

 

microscopy [41–45]. Since the eigenvalues of $H_0$ are bounded, we can perform a shifting and a rescaling on $H_0$ such that $E_{\mathrm{GS}} = 0$ and the eigenvalues lie in [0, 1). In such case, $\rho(E \in [0,1), l)$ is a bounded single-variable function for fixed $l$, which is a crucial property that allows it to be expanded in Chebyshev polynomials $T_n(E) = \cos(n \arccos E)$:

$$\rho(E,l) = \frac{1}{\pi\sqrt{1-E^2}}\left(\mu_0 + 2\sum_{n=1}^{\infty}\mu_n T_n(E)\right) \tag{2}$$

where the coefficients satisfy $\mu_n = \int_{-1}^{1} dE \rho(E,l) T_n(E) = \langle \mathrm{GS}|S_l^- T_n(H_0) S_l^+|\mathrm{GS}\rangle + \langle \mathrm{GS}|S_l^+ T_n(H_0) S_l^-|\mathrm{GS}\rangle$. Using the recursion relation of Chebyshev polynomials $T_{n+1}(x) = 2xT_n(x) - T_{n-1}(x)$, the first term of $\mu_n$ can be computed as $\mu_n = \langle v|v_n\rangle$ where $|v\rangle = S_l^+|\mathrm{GS}\rangle$ and

$$\begin{aligned} |v_{n+1}\rangle &= 2H_0|v_n\rangle - |v_{n-1}\rangle \\ |v_0\rangle &= |v\rangle, \quad |v_1\rangle = H_0|v\rangle, \end{aligned} \tag{3}$$

and similarly for the second term. The recursive structure of Eq. (3) allows the efficient computation of $\mu_n$ and $\rho(E,l)$. Furthermore, its simple algebraic structure allows it to be implemented with MPS representation of states, where the ground state can be computed with DMRG. Finally, Eq. (2) is approximated with a truncation of the summation to $N$th order, where a Jackson kernel $g_n^N = \{[(N-n+1)\cos\frac{n\pi}{N+1} + \sin\frac{n\pi}{N+1}\cot\frac{\pi}{N+1}]/(N+1)\}$ is multiplied to the coefficients $\mu_n$ to damp Gibbs oscillations [36].

We now generalize Eq. (1) to an open spin system described with an effective NH spin Hamiltonian $H$. Unlike a Hermitian Hamiltonian, a NH Hamiltonian generally has a complex spectrum $\{E_n \in \mathbb{C}\}$. In addition, the left eigenvector $|\Psi_{L,n}\rangle$ and the right eigenvector $|\Psi_{R,n}\rangle$ corresponding to the same eigenvalue $E_n$ of $H$ are generally different and satisfy $\langle \Psi_{L,m}|\Psi_{R,n}\rangle = \delta_{mn}$. The eigendecomposition of $H$ is $H = \sum_n E_n |\Psi_{R,n}\rangle\langle\Psi_{L,n}|$. Thus, we define the local dynamical spin correlator as

$$\begin{aligned} \mathcal{S}(\omega,l) = &\langle \mathrm{GS}_L|S_l^-\delta^2(\omega + E_{\mathrm{GS}} - H)S_l^+|\mathrm{GS}_R\rangle \\ &+\langle \mathrm{GS}_L|S_l^+\delta^2(\omega + E_{\mathrm{GS}} - H)S_l^-|\mathrm{GS}_R\rangle, \end{aligned} \tag{4}$$

where $\omega$ is a complex number, $|\mathrm{GS}_{\mathrm{L,R}}\rangle$ are left and right eigenvectors corresponding to the eigenvalue of smallest real part [29,46], and $\delta^2(\omega - H) = \sum_n \delta(\Re(\omega - E_n))\delta(\Im(\omega - E_n))|\Psi_{R,n}\rangle\langle\Psi_{L,n}|$. Since $\omega$ is complex, $\mathcal{S}(\omega,l)$ is no longer a function of a single variable, and does not have the Chebyshev expansion Eq. (2) that allows it to be computed with the KPM [47].

We now present how a NHKPM algorithm [48] allows us to efficiently compute Eq. (4), and more generally, generic spectral functions of the form

$$f(\omega) = \langle \psi_L|\delta^2(\omega - H)|\psi_R\rangle, \tag{5}$$

where $|\psi_L\rangle, |\psi_R\rangle$ are arbitrary states. The key observation is, although Eq. (5) cannot be computed with the KPM directly, it can be related to the spectral functions of the Hermitrized form of $\omega - H$:

$$\mathcal{H} = \begin{pmatrix} & \omega - H \\ \omega^* - H^\dagger & \end{pmatrix}. \tag{6}$$

In particular, using $\partial_{\omega^*}(1/\omega) = \pi\delta(\Re(\omega))\delta(\Im(\omega))$ [56], we can rewrite Eq. (5) as

$$f(\omega) = \frac{1}{\pi}\partial_{\omega^*} G(E=0) \tag{7}$$

where $G(E) = \langle L|(E - \mathcal{H})^{-1}|R\rangle$ is the Green's function of $\mathcal{H}$ with $|L\rangle = \binom{0}{|\psi_L\rangle}$ and $|R\rangle = \binom{|\psi_R\rangle}{0}$. Since $\mathcal{H}$ is Hermitian, its Green's function $G(E)$ has the Chebyshev expansion Eq. (2), resulting in an expansion of $f(\omega)$ in Chebyshev polynomials of $\mathcal{H}$:

$$f(\omega) = \frac{2}{\pi^2}\sum_{n=1}^{\infty}(-1)^{n+1}\langle L|\partial_{\omega^*} T_{2n-1}(\mathcal{H})|R\rangle \tag{8}$$

with the recursion relation $\partial_{\omega^*} T_{n+1}(\mathcal{H}) = 2\binom{0\,0}{1\,0} T_n(\mathcal{H}) + 2\mathcal{H}\partial_{\omega^*} T_n(\mathcal{H}) - \partial_{\omega^*} T_{n-1}(\mathcal{H})$. Finally, the above recursion relation on $T_n(\mathcal{H})$ is transformed into an update of vectors, similar to Eq. (3), allowing $f(\omega)$ to be computed with the KPM. We use a MPS representation for the states $S_l^\pm|\mathrm{GS}_{\mathrm{L,R}}\rangle$ in the computation of Eq. (4), which enables computation for large size systems. We use a Krylov-Schur algorithm [57] to compute the states with the smallest real part [58].

We now use the NHKPM to identify the topological end modes emerging in a NH many-body system. We take the following NH $S = 1/2$ chain with antiferromagnetic exchange $J = 1$ [Fig. 1(a)]:

$$\begin{aligned} H = &\sum_{l=1}^{L-1}\left(\frac{J+\gamma}{2}S_l^+ S_{l+1}^- + \frac{J-\gamma}{2}S_l^- S_{l+1}^+ + J_z S_l^z S_{l+1}^z\right) \\ &+ \sum_{l=1}^{L} i h_l^z S_l^z \end{aligned} \tag{9}$$

where $h_l^z = -h_z$ if $l \bmod 4 = 2, 3$ and $h_l^z = 0$ otherwise. It is first illustrative to perform a Jordan-Wigner transformation to Eq. (9), leading to a NH interacting spinless fermion model:

$$\begin{aligned} \tilde{H} = &\sum_{l=1}^{L-1}\left[\frac{J+\gamma}{2}c_l^\dagger c_{l+1} + \frac{J-\gamma}{2}c_{l+1}^\dagger c_l \right. \\ &\left. + J_z\left(c_l^\dagger c_l - \frac{1}{2}\right)\left(c_{l+1}^\dagger c_{l+1} - \frac{1}{2}\right)\right] + \sum_{l=1}^{L} i h_l^z\left(c_l^\dagger c_l - \frac{1}{2}\right). \end{aligned} \tag{10}$$

When $J_z = 0$, Eq. (10) becomes a noninteracting spinless fermion model, which for $\gamma = 0$ and nonzero $h_z$ is known to give rise to topological end states whose real part of the energy is 0 [59]. The bulk topology of this model is characterized by a hidden Chern number which faithfully predicts the number of stable end states with purely imaginary energy [59,60]. It has been shown that in the presence of a finite interaction $J_z$, a sufficiently large $h_z$ would still give rise to the topological end states [61]. In the following we explore the non-Hermitian many-body topology of the model via computing dynamical excitations using the NHKPM algorithm, both in the absence and presence of the NHSE. For concreteness we take $J_z = 1/2J$, yet analogous results can be obtained for general values of $J_z$.

We first focus on a chain of length $L = 8$ in which we can implement the NHKPM exactly with exact diagonalization as a benchmark. We first compute the total dynamical spin correlator, defined as

$$\tilde{\mathcal{S}}_{\mathrm{tot}}(\omega) = \left| \sum_{l=1}^{L} \mathcal{S}(\omega, l) \right| \tag{11}$$

where $\mathcal{S}(\omega, l)$ is defined in Eq. (4) [62]. The total dynamical spin correlator reveals the energy of the states that have finite overlap with the ground state with one $S_z = \pm 1$ excitation. We see that as $h_z$ increases, the real part of the energy of the lowest excited states is shifted towards 0, whereas the higher states are shifted away from 0 [Figs. 1(b)–1(d)]. To see if the lowest excited states are topological end states, we compute the projected local dynamical structure factor, defined as

$$\tilde{\rho}(E \in \mathbb{R}, l) = \left| \int \mathcal{S}(E + iy, l) dy \right|. \tag{12}$$

This quantity identifies the local spectral density of $S_z = \pm 1$ excitations at a given real energy $E$. In particular, when $H$ is Hermitian, $\tilde{\rho}(E, l)$ is reduced to the local spin structure factor defined in Eq. (1). Figures 1(e)–1(g) show $\tilde{\rho}(E, l)$ for different values of $h_z$, we see that for $h_z = 0$ the lowest states show nonvanishing spectral density in the bulk. As $h_z$ increases to $h_z = J$ the spectral density in the bulk reduces, and eventually for sufficiently large $h_z = 2J$ the states become localized at the ends, reflecting the nontrivial line topology in the bulk. Because of the short chain length, finite-size effects prevent clearly observing topological end states for $h_z = J$ due to hybridization.

To approach the thermodynamic limit and demonstrate the capabilities of the NHKPM algorithm, we now move on to consider a chain of length $L = 24$. As these systems are too large to be treated by exact diagonalization, we now use a full tensor-network implementation with the MPS in the NHKPM algorithm. The total dynamical spin correlator $\tilde{\mathcal{S}}_{\mathrm{tot}}(\omega)$ and the projected local dynamical structure factor

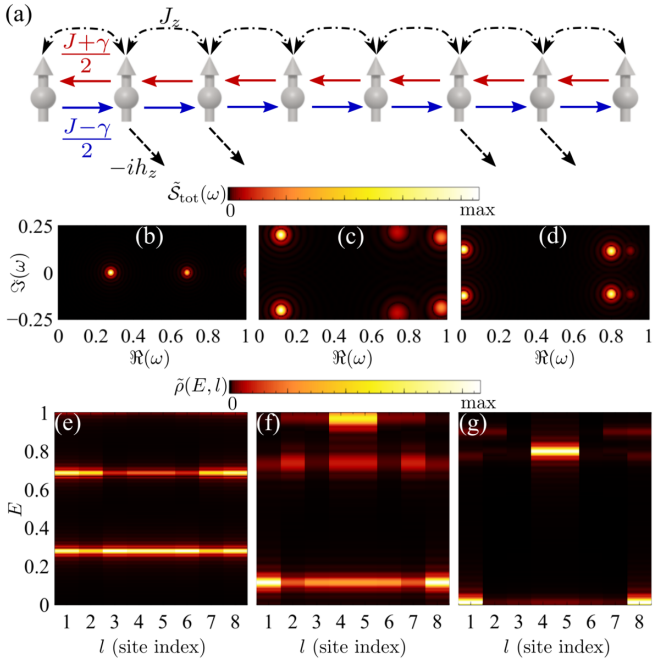


FIG. 1. (a) Sketch of the model Hamiltonian $H$ in Eq. (9). (b)–(d) Total dynamical spin correlator $\tilde{\mathcal{S}}_{\mathrm{tot}}(\omega)$ of $H$ with $L = 8$, $\gamma = 0$ and (b) $h_z = 0$, (c) $h_z = J$, (d) $h_z = 2J$. (e)–(g) Projected local dynamical structure factor $\tilde{\rho}(E, l)$ corresponding to cases (b)–(d), respectively. Topological spin excitations with almost zero real energy are revealed in (g).

$\tilde{\rho}(E, l)$ are computed for $h_z = 0$ and $h_z = J$ in this case (Fig. 2). We see from Figs. 2(a) and 2(b) that for $h_z = J$ there are clearly two states close to 0 real energy, and are isolated from the higher states with a line gap, whereas for $h_z = 0$ there is no such behavior. From Figs. 2(c) and 2(d) we can observe the topological end states for $h_z = J$, whereas for $h_z = 0$ the lowest states are mainly distributed in the bulk. These show that the model Eq. (9) is not topological for $h_z = 0$, and is topological for $h_z = J$ even in the presence of many-body interactions.

We now consider a finite $\gamma$ term, which is known to give rise to the NHSE [4–6]. In the noninteracting limit, the spectrum of $H$ in the presence of the NHSE is known to be drastically different under different boundary conditions: in the thermodynamic limit; the spectrum of $H$ is purely real under the open boundary condition (OBC), and features a point gap under the periodic boundary condition (PBC). On the contrary, the spectrum of the Hermitrized Hamiltonian $\mathcal{H}$ is not sensitive to boundary conditions: in the thermodynamic limit, the spectrum is the same under both boundary conditions except that when $\omega$ lies in the point gap of $H$, the spectrum under the OBC shows more topological zero modes than that under the PBC [16,63]. It is due to the contribution of these additional zero modes to the Green's function of $\mathcal{H}$ in Eq. (7) that faithfully computing the spectral function of H using NHKPM [64] is allowed, despite the different sensitivities of the spectral

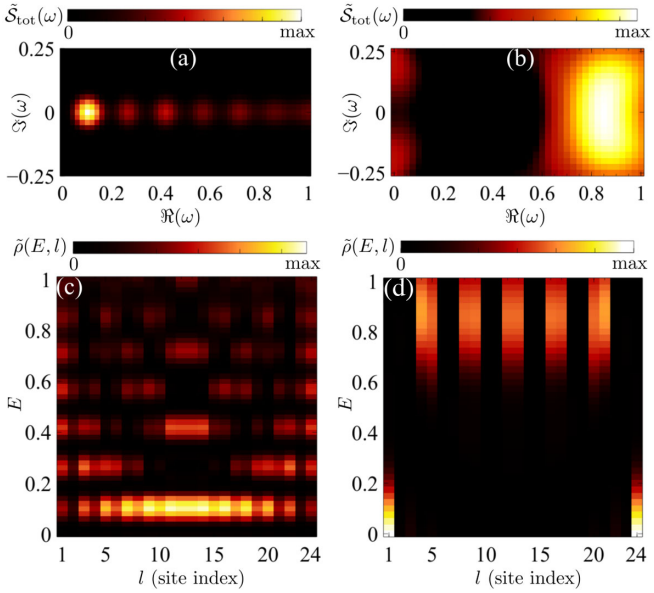


FIG. 2. (a) and (b) Total dynamical spin correlator $\tilde{\mathcal{S}}_{\rm tot}(\omega)$ of $H$ defined in Eq. (9) with $L = 24$, $\gamma = 0$ and (a) $h_z = 0$ and (b) $h_z = J$. $\tilde{\mathcal{S}}_{\rm tot}(\omega)$ reveals a many-body line gap in (b). (c) and (d) Projected local dynamical structure factor $\tilde{\rho}(E, l)$ corresponding to cases (a),(b), respectively. $\tilde{\rho}(E, l)$ reveals topological many-body excitations in (d), indicating that the line gap in (b) is topological.

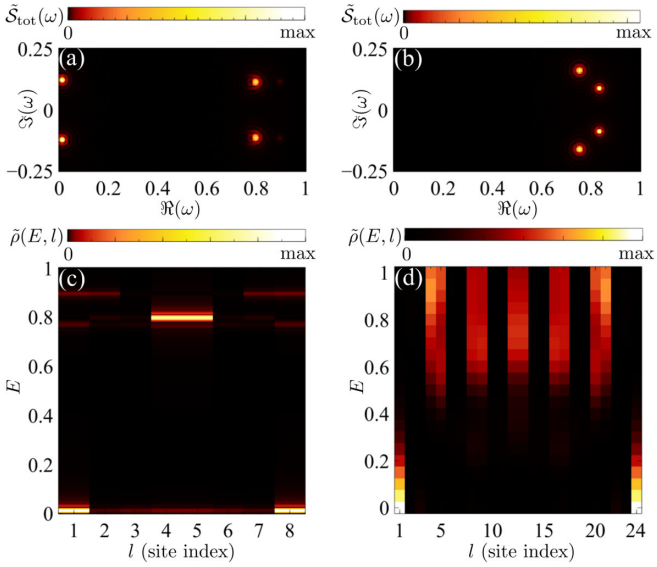


FIG. 3. (a),(b) Total dynamical spin correlator $\tilde{\mathcal{S}}_{\rm tot}(\omega)$ of $H$ defined in Eq. (9) with $L = 8$, $h_z = 2J$ and $\gamma = 0.1J$ under (a) open boundary condition and (b) periodic boundary condition. (c) Projected local dynamical structure factor $\tilde{\rho}(E, l)$ corresponding to (a), showing the persistence of topological end modes in the presence of the NHSE. (d) $\tilde{\rho}(E, l)$ of $H$ with $L = 24$, $h_z = J$ and $\gamma = 0.1J$, showing the topological end modes in the presence of the NHSE for a longer chain.

functions of $H$ and $\mathcal{H}$ to the boundary condition. In the interacting case, the spectrum of $H$ has no point gaps in the thermodynamic limit, and the above analysis no longer holds. Thus, it is unclear whether the algorithm allows for comparable accuracy, which we examine below. It is worth noting that the case $\gamma < J$ reduces to $\gamma = 0$ under a similarity transformation to $H$:

$$T = e^{\sum_l l\alpha S_l^z}, \qquad \alpha = \ln r, \qquad r = \sqrt{\frac{J+\gamma}{J-\gamma}}$$
$$TH(J, \gamma, J_z, h_z)T^{-1} = H'(J', 0, J_z, h_z). \tag{13}$$

The new uniform exchange is $J' = \sqrt{(J+\gamma)(J-\gamma)}$ which is approximately $J$ for $\gamma = 0.1J$. This similarity transformation changes the spectral function Eq. (4) for $H$ to the same spectral function for $H'$, leading to dynamical correlators analogous to the $\gamma = 0$ case for $\gamma \ll J$. As a benchmark, we compute both $\tilde{\mathcal{S}}_{\rm tot}(\omega)$ and $\tilde{\rho}(E, l)$ for $H$ with $L = 8$, $h_z = 2J$, and $\gamma = 0.1J$ under the OBC [Figs. 3(a) and 3(c)], where the results are analogous to Figs. 1(d) and 1(g), demonstrating that the NHKPM faithfully computes both spectral functions. We also show $\tilde{\mathcal{S}}_{\rm tot}(\omega)$ for $H$ under the same set of parameters under the PBC, where faithful results are obtained: the two end states with almost 0 real energy under the OBC vanish under the PBC. We also compute $\tilde{\rho}(E, l)$ for a longer chain with $L = 24$, $h_z = J$, and $\gamma = 0.1J$ [Fig. 3(d)], where analogous results to Fig. 2(d) are obtained. This demonstrates the capability of the NHKPM to compute spectral functions and identify topological edge modes in the presence of the NHSE. We note that in the presence of the NHSE, bulk states become also localized at the edge. In this case, it is the definition of the local dynamical spin correlator in Eq. (4) that allows us to distinguish edge states from bulk states, and image edge modes in real space. Another remark is that in the presence of the NHSE, the condition number [66] of $H$ increases exponentially. Therefore, numerically determining the exact spectrum of a Hamiltonian with the NHSE is often very hard and time-consuming. In our algorithm, by using Eq. (7), this hard task is converted to the computation of the Green's function of a Hermitian Hamiltonian, which is relatively more controllable.

We now comment on several future perspectives for the NHKPM algorithm. It is worth noting that in some NH systems the physically relevant state could be the state with the largest imaginary energy, which is the steady state of the system after a long time evolution. The algorithm could identify the energy of many-body excitations near that state, and applies efficiently as long as the state is not highly entangled. In addition to addressing topology, the NHKPM algorithm can also address the (higher-order) NHSE [67] by computing spectral functions defined in a basis of solely left (right) eigenvectors, or by computing the Green's function [68]. Finally, we note while our algorithm is implemented within the MPS formalism, this methodology can be extended to more generic tensor-network

algorithms [69,70] and neural-network quantum states [71,72]. Such extensions would allow tackling many-body interacting two-dimensional non-Hermitian problems.

To summarize, we developed a NHKPM algorithm that can efficiently compute local spectral functions in a NH many-body model. In particular, we showed that this methodology allows us to compute local dynamical spin correlators in a non-Hermitian interacting system featuring topological excitations, directly allowing us to image the topological end modes in real and frequency space. We further showed that this algorithm works in the presence of the non-Hermitian skin effect. Our results put forward a new method to efficiently compute spectral functions of non-Hermitian many-body systems of large sizes beyond the capability of exact diagonalization, and make an essential step toward the critical open problem of addressing nontrivial topology in non-Hermitian many-body systems.

We acknowledge the computational resources provided by the Aalto Science-IT project, and the financial support from the Academy of Finland Projects No. 331342 and No. 336243 and the Jane and Aatos Erkko Foundation. We thank Z. Wang, S. Sayyad, T. Hyart, M. Niedermeier, and P. Vecsei for fruitful discussions. The numerical calculations are done with the ITENSOR library [73].

*songf18@mails.tsinghua.edu.cn
†jose.lado@aalto.fi

[1] H. Breuer and F. Petruccione, *The Theory of Open Quantum Systems* (Oxford University Press, Oxford, 2002).
[2] E. J. Bergholtz, J. C. Budich, and F. K. Kunst, Exceptional topology of non-hermitian systems, Rev. Mod. Phys. **93**, 015005 (2021).
[3] Y. Ashida, Z. Gong, and M. Ueda, Non-hermitian physics, Adv. Phys. **69**, 249 (2020).
[4] S. Yao and Z. Wang, Edge States and Topological Invariants of Non-Hermitian Systems, Phys. Rev. Lett. **121**, 086803 (2018).
[5] C. H. Lee and R. Thomale, Anatomy of skin modes and topology in non-hermitian systems, Phys. Rev. B **99**, 201103(R) (2019).
[6] F. K. Kunst, E. Edvardsson, J. C. Budich, and E. J. Bergholtz, Biorthogonal Bulk-Boundary Correspondence in Non-Hermitian Systems, Phys. Rev. Lett. **121**, 026808 (2018).
[7] L. Xiao, T. Deng, K. Wang, G. Zhu, Z. Wang, W. Yi, and P. Xue, Non-hermitian bulk–boundary correspondence in quantum dynamics, Nat. Phys. **16**, 761 (2020).
[8] T. Helbig, T. Hofmann, S. Imhof, M. Abdelghany, T. Kiessling, L. W. Molenkamp, C. H. Lee, A. Szameit, M. Greiter, and R. Thomale, Generalized bulk–boundary correspondence in non-hermitian topolectrical circuits, Nat. Phys. **16**, 747 (2020).
[9] S. Weidemann, M. Kremer, T. Helbig, T. Hofmann, A. Stegmaier, M. Greiter, R. Thomale, and A. Szameit, Topological funneling of light, Science **368**, 311 (2020).
[10] A. Ghatak, M. Brandenbourger, J. van Wezel, and C. Coulais, Observation of non-hermitian topology and its bulk-edge correspondence in an active mechanical metamaterial, Proc. Natl. Acad. Sci. U.S.A. **117**, 29561 (2020).
[11] T. E. Lee, Anomalous Edge State in a Non-Hermitian Lattice, Phys. Rev. Lett. **116**, 133903 (2016).
[12] V. M. Martinez Alvarez, J. E. Barrios Vargas, and L. E. F. Foa Torres, Non-hermitian robust edge states in one dimension: Anomalous localization and eigenspace condensation at exceptional points, Phys. Rev. B **97**, 121401(R) (2018).
[13] Z. Gong, Y. Ashida, K. Kawabata, K. Takasan, S. Higashikawa, and M. Ueda, Topological Phases of Non-Hermitian Systems, Phys. Rev. X **8**, 031079 (2018).
[14] K. Kawabata, K. Shiozaki, M. Ueda, and M. Sato, Symmetry and Topology in Non-Hermitian Physics, Phys. Rev. X **9**, 041015 (2019).
[15] H. Zhou and J. Y. Lee, Periodic table for topological bands with non-hermitian symmetries, Phys. Rev. B **99**, 235112 (2019).
[16] N. Okuma, K. Kawabata, K. Shiozaki, and M. Sato, Topological Origin of Non-Hermitian Skin Effects, Phys. Rev. Lett. **124**, 086801 (2020).
[17] K. Zhang, Z. Yang, and C. Fang, Correspondence Between Winding Numbers and Skin Modes in Non-Hermitian Systems, Phys. Rev. Lett. **125**, 126402 (2020).
[18] D. S. Borgnia, A. J. Kruchkov, and R.-J. Slager, Non-Hermitian Boundary Modes and Topology, Phys. Rev. Lett. **124**, 056802 (2020).
[19] C. M. Bender and S. Boettcher, Real Spectra in Non-Hermitian Hamiltonians Having *PT* Symmetry, Phys. Rev. Lett. **80**, 5243 (1998).
[20] C. M. Bender, Making sense of non-hermitian Hamiltonians, Rep. Prog. Phys. **70**, 947 (2007).
[21] R. El-Ganainy, K. G. Makris, M. Khajavikhan, Z. H. Musslimani, S. Rotter, and D. N. Christodoulides, Non-hermitian physics and *PT* symmetry, Nat. Phys. **14**, 11 (2018).
[22] W. D. Heiss, Exceptional points of non-hermitian operators, J. Phys. A **37**, 2455 (2004).
[23] M. V. Berry, Physics of nonhermitian degeneracies, Czech. J. Phys. **54**, 1039 (2004).
[24] M.-A. Miri and A. Alù, Exceptional points in optics and photonics, Science **363**, eaar7709 (2019).
[25] Ş. K. Özdemir, S. Rotter, F. Nori, and L. Yang, Parity-time symmetry and exceptional points in photonics, Nat. Mater. **18**, 783 (2019).
[26] S.-B. Zhang, M. M. Denner, and T. C. V. Bzdušek, M. A. Sentef, and T. Neupert, Symmetry breaking and spectral structure of the interacting Hatano-Nelson model, Phys. Rev. B **106**, L121102 (2022).
[27] D. J. Luitz and F. Piazza, Exceptional points and the topology of quantum many-body spectra, Phys. Rev. Res. **1**, 033051 (2019).
[28] R. Schäfer, J. C. Budich, and D. J. Luitz, Symmetry protected exceptional points of interacting fermions, Phys. Rev. Res. **4**, 033181 (2022).
[29] K. Kawabata, K. Shiozaki, and S. Ryu, Many-body topology of non-hermitian systems, Phys. Rev. B **105**, 165137 (2022).

[30] F. Alsallom, L. Herviou, O. V. Yazyev, and M. Brzezińska, Fate of the non-hermitian skin effect in many-body fermionic systems, Phys. Rev. Res. **4**, 033122 (2022).

[31] S. R. White, Density Matrix Formulation for Quantum Renormalization Groups, Phys. Rev. Lett. **69**, 2863 (1992).

[32] T. D. Kühner and S. R. White, Dynamical correlation functions using the density matrix renormalization group, Phys. Rev. B **60**, 335 (1999).

[33] E. Jeckelmann, Dynamical density-matrix renormalization-group method, Phys. Rev. B **66**, 045114 (2002).

[34] S. R. White and A. E. Feiguin, Real-Tame Evolution Using the Density Matrix Renormalization Group, Phys. Rev. Lett. **93**, 076401 (2004).

[35] J. Haegeman, J. I. Cirac, T. J. Osborne, and I. Pižorn, H. Verschelde, and F. Verstraete, Time-Dependent Variational Principle for Quantum Lattices, Phys. Rev. Lett. **107**, 070601 (2011).

[36] A. Weiße, G. Wellein, A. Alvermann, and H. Fehske, The kernel polynomial method, Rev. Mod. Phys. **78**, 275 (2006).

[37] F. A. Wolf, I. P. McCulloch, O. Parcollet, and U. Schollwöck, Chebyshev matrix product state impurity solver for dynamical mean-field theory, Phys. Rev. B **90**, 115124 (2014).

[38] J. L. Lado and O. Zilberberg, Topological spin excitations in Harper-Heisenberg spin chains, Phys. Rev. Res. **1**, 033009 (2019).

[39] N. Hatano and J. Feinberg, Chebyshev-polynomial expansion of the localization length of hermitian and non-hermitian random chains, Phys. Rev. E **94**, 063305 (2016).

[40] The source codes are available on https://github.com/GUANGZECHEN/NHKPM.jl.

[41] A. J. Heinrich, J. A. Gupta, C. P. Lutz, and D. M. Eigler, Single-atom spin-flip spectroscopy, Science **306**, 466 (2004).

[42] A. Spinelli, B. Bryant, F. Delgado, J. Fernández-Rossier, and A. F. Otte, Imaging of spin waves in atomically designed nanomagnets, Nat. Mater. **13**, 782 (2014).

[43] S. Baumann, W. Paul, T. Choi, C. P. Lutz, A. Ardavan, and A. J. Heinrich, Electron paramagnetic resonance of individual atoms on a surface, Science **350**, 417 (2015).

[44] K. Yang, Y. Bae, W. Paul, F. D. Natterer, P. Willke, J. L. Lado, A. Ferrón, T. Choi, J. Fernández-Rossier, A. J. Heinrich, and C. P. Lutz, Engineering the Eigenstates of Coupled Spin-1/2 Atoms on a Surface, Phys. Rev. Lett. **119**, 227206 (2017).

[45] S. Kezilebieke, R. Žitko, M. Dvorak, T. Ojanen, and P. Liljeroth, Observation of coexistence of yu-shiba-rusinov states and spin-flip excitations, Nano Lett. **19**, 4614 (2019).

[46] S.-B. Zhang, M. M. Denner, T. Bzdušek, M. A. Sentef, and T. Neupert, Symmetry breaking and spectral structure of the interacting hatano-nelson model, Phys. Rev. B **106**, L121102 (2022).

[47] There exists a multi-variable Chebyshev expansion for $f(\omega)$, yet the coefficients in such case cannot be computed efficiently as in Eq. (3) [36].

[48] See Supplemental Material at http://link.aps.org/supplemental/10.1103/PhysRevLett.130.100401 for the technical details of our algorithm and the analysis of the numerical complexity of our algorithm. References [49–55] are included in the Supplemental Material.

[49] H. G. Dawson, On the numerical value of $\int_0^h \exp(x^2)dx$, Proc. London Math. Soc. **s1-29**, 519 (1897).

[50] N. Okuma and M. Sato, Hermitian zero modes protected by nonnormality: Application of pseudospectra, Phys. Rev. B **102**, 014203 (2020).

[51] U. Schollwöck, The density-matrix renormalization group in the age of matrix product states, Ann. Phys. (N.Y.) **326**, 96 (2011), january 2011 Special Issue.

[52] T. Enss and U. Schollwöck, On the choice of the density matrix in the stochastic TMRG, J. Phys. A **34**, 7769 (2001).

[53] G. K.-L. Chan and T. Van Voorhis, Density-matrix renormalization-group algorithms with nonorthogonal orbitals and non-hermitian operators, and applications to polyenes, J. Chem. Phys. **122**, 204101 (2005).

[54] D.-W. Zhang, Y.-L. Chen, G.-Q. Zhang, L.-J. Lang, Z. Li, and S.-L. Zhu, Skin superfluid, topological mott insulators, and asymmetric dynamics in an interacting non-hermitian Aubry-André-Harper model, Phys. Rev. B **101**, 235150 (2020).

[55] K. Yamamoto, M. Nakagawa, M. Tezuka, M. Ueda, and N. Kawakami, Universal properties of dissipative tomonaga-luttinger liquids: Case study of a non-hermitian XXZ spin chain, Phys. Rev. B **105**, 205125 (2022).

[56] J. Feinberg and A. Zee, Non-hermitian random matrix theory: Method of hermitian reduction, Nucl. Phys. **B504**, 579 (1997).

[57] G. W. Stewart, A Krylov-Schur algorithm for large Eigen problems, SIAM J. Matrix Anal. Appl. **23**, 601 (2002).

[58] The fidelity of these states are verified in the Supplemental Material [48], in section "Fidelity of ground states computed with the Krylov-Schur Algorithm."

[59] W. Brzezicki and T. Hyart, Hidden chern number in one-dimensional non-hermitian chiral-symmetric systems, Phys. Rev. B **100**, 161105(R) (2019).

[60] K. Kawabata, K. Shiozaki, M. Ueda, and M. Sato, Symmetry and Topology in Non-Hermitian Physics, Phys. Rev. X **9**, 041015 (2019).

[61] T. Hyart and J. L. Lado, Non-hermitian many-body topological excitations in interacting quantum dots, Phys. Rev. Res. **4**, L012006 (2022).

[62] We take the absolute value in Eq. (11) since $\mathcal{S}(\omega, l)$ is no longer real-valued in this case.

[63] L. Herviou, J. H. Bardarson, and N. Regnault, Defining a bulk-edge correspondence for non-hermitian Hamiltonians via singular-value decomposition, Phys. Rev. A **99**, 052118 (2019).

[64] We demonstrate this with the Hatano-Nelson model [65] in the Supplemental Material [48], in section "Total density of states in Hatano-Nelson model with NHKPM".

[65] N. Hatano and D. R. Nelson, Localization Transitions in Non-Hermitian Quantum Mechanics, Phys. Rev. Lett. **77**, 570 (1996).

[66] D. Belsley, E. Kuh, and R. Welsch, *Regression Diagnostics: Identifying Influential Data and Sources of Collinearity*, Wiley Series in Probability and Statistics (Wiley, New York, 2005).

[67] K. Kawabata, M. Sato, and K. Shiozaki, Higher-order non-hermitian skin effect, Phys. Rev. B **102**, 205118 (2020).

[68] W.-T. Xue, M.-R. Li, Y.-M. Hu, F. Song, and Z. Wang, Simple formulas of directional amplification from non-bloch band theory, Phys. Rev. B **103**, L241408 (2021).

[69] J. I. Cirac, D. Pérez-García, N. Schuch, and F. Verstraete, Matrix product states and projected entangled pair states:

Concepts, symmetries, theorems, Rev. Mod. Phys. **93**, 045003 (2021).

[70] R. Orús, A practical introduction to tensor networks: Matrix product states and projected entangled pair states, Ann. Phys. (N.Y.) **349**, 117 (2014).

[71] G. Carleo and M. Troyer, Solving the quantum many-body problem with artificial neural networks, Science **355**, 602 (2017).

[72] D. Hendry, H. Chen, P. Weinberg, and A. E. Feiguin, Chebyshev expansion of spectral functions using restricted Boltzmann machines, Phys. Rev. B **104**, 205130 (2021).

[73] M. Fishman, S. R. White, and E. M. Stoudenmire, The ITensor software library for tensor network calculations, arXiv:2007.14822.